Supporting Information

Regulating NO_2 adsorption at ambient temperature by manipulating copper species as binding sites in copper-modified SSZ-13 zeolites

Mingzhe Sun,‡[a,b] Tianqi Wang,‡[a,b] Calvin Ku,[a] Aamir Hanif,[a,b] Tian Tian,[c] Bernt Johannessen,[d,e] Qinfen Gu,*[d] Ziyi Li,*[f] Patrick Sit,*[a] and Jin Shang,*[a,b,g]

[a] *School of Energy and Environment, City University of Hong Kong, Tat Chee Avenue, Kowloon, Hong Kong SAR, P.R. China. E-mail: jinshang@cityu.edu.hk; patrick.h.sit@cityu.edu.hk*

[b] *City University of Hong Kong Shenzhen Research Institute, Nanshan District, Shenzhen 518000, P.R. China.*

[c] *Department of Applied Biology and Chemical Technology, The Hong Kong Polytechnic University, Hung Hom, Hong Kong SAR, P.R. China.*

[d] *Australian Synchrotron, ANSTO, 800 Blackburn Road, Clayton, VIC 3168, Australia. E-mail: qinfeng@ansto.gov.au*

[e] *Institute for Superconducting & Electronic Materials, University of Wollongong, Wollongong, NSW 2522, Australia.*

[f] *School of Energy and Environmental Engineering, University of Science and Technology Beijing, Beijing 100083, China. E-mail: ziyili@ustb.edu.cn*

[g] *Low-Carbon and Climate Impact Research Center, School of Energy and Environment, City University of Hong Kong, Hong Kong SAR*

‡These authors contributed equally to this work.

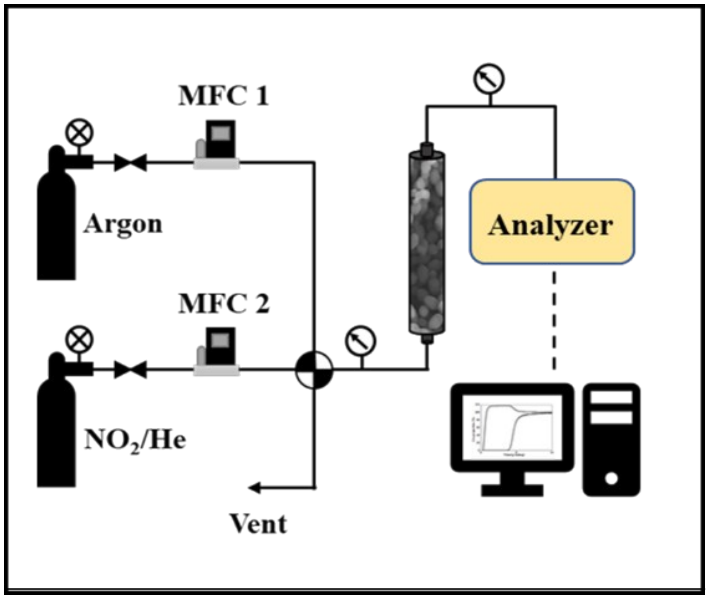

Figure S1. Schematic diagram of the setup use for dynamic column breakthrough (DCB) experiments.

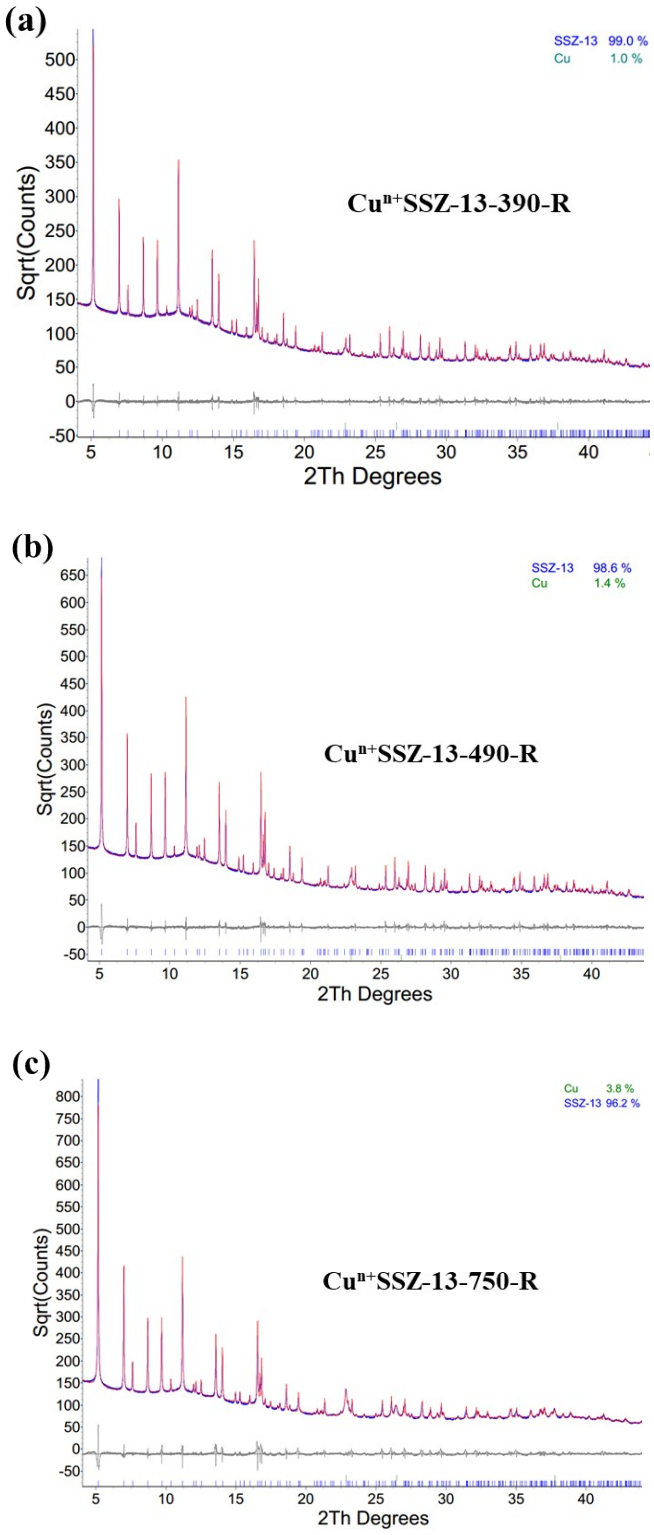

Figure S2. Rietveld refinement of synchrotron X-ray powder diffraction of the Cu^{n+}SSZ-13 samples reduced 390, 490 and 750 ^{o}C. Red line corresponds to the data points, and blue line denotes the calculated pattern. The difference is shown by the grey line. The calculated positions of Bragg reflections are marked by blue vertical ticks at the bottom. The green vertical ticks are the diffractions of Cu.

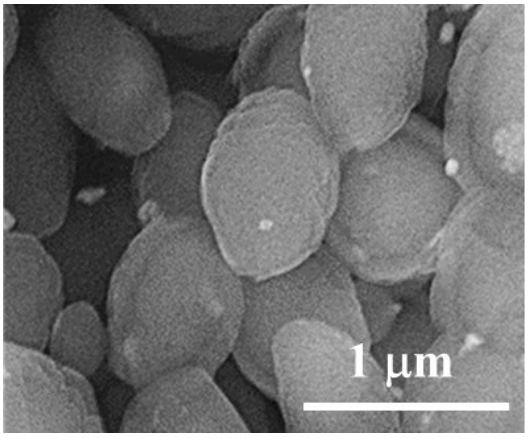

Figure S3. SEM image of Cu^{n+}SSZ-13-250-R.

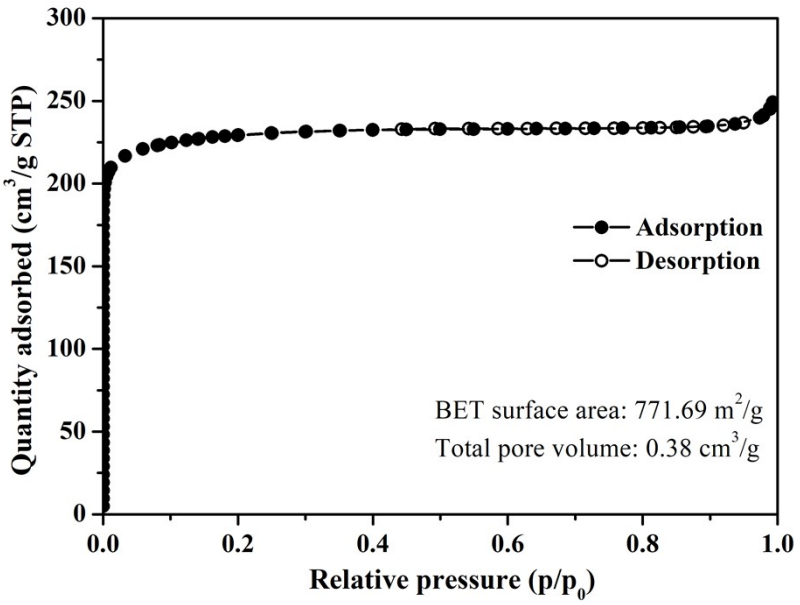

Figure S4. N_2 adsorption-desorption isotherms of H^+SSZ-13 at -196 ^oC.

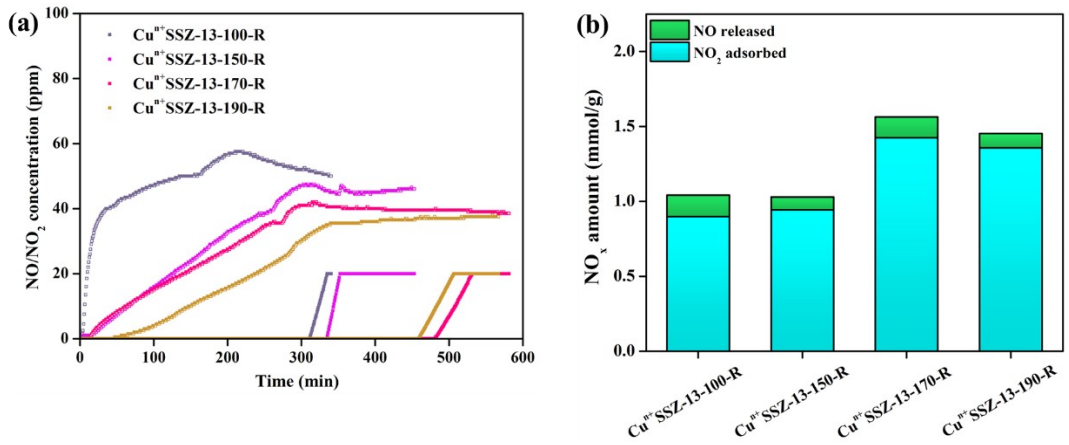

Figure S5. (a) NO_2 (1000 ppm) dynamic adsorption at room temperature on $Cu^{n+}SSZ$-13 samples without thermal activation. The hollow (□) and solid (■) dots represent the concentration of NO and NO_2, respectively. **(b)** The corresponding NO_2 adsorption capacity and NO released amount.

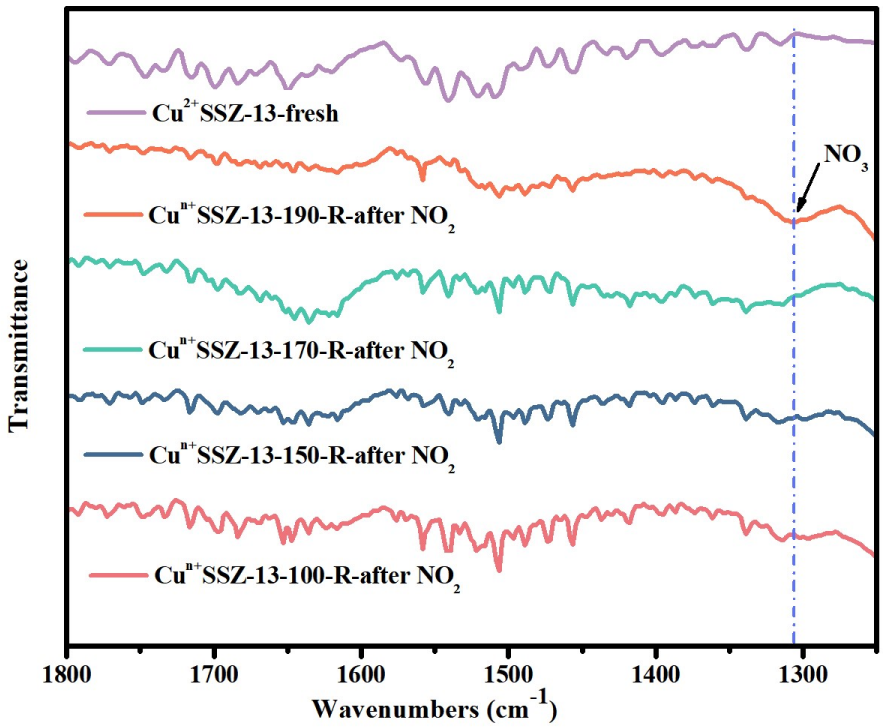

Figure S6. FTIR spectra of fresh Cu^{2+}SSZ-13 and Cu^{n+}SSZ-13 samples after NO_2 adsorption.

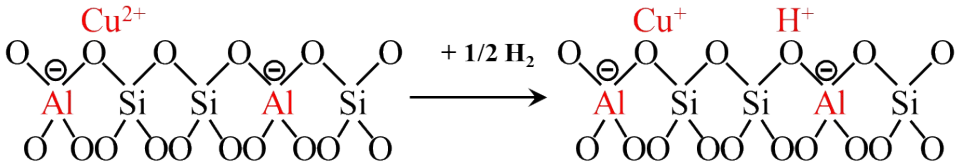

Figure S7. Illustration of the evolution of the zeolite cationic sites during H_2 reduction.

After H_2 reduction, the cation amount ($N_{after} = n(Cu^+) + n(H^+)$) is double of that before the reduction ($N_{before} = n(Cu^{2+})$).

Table S1. Comparison of NO_2 adsorption capacity of SSZ-13 zeolites modified with different metals.

Adsorbent	NO_2 concentration (ppm)	Temperature (°C)	NO_2 adsorption (mmol/g)	Ref.
Pd/SSZ-13	15	120	2.57×10^{-3}	1
Pd/SSZ-13	24	120	4.86×10^{-3}	1
Fe-BEA	1000	200	4.47×10^{-2}	2
Cu-CHA	1000	200	8.06×10^{-2}	2
Cu^{n+}SSZ-13	1000	25	1.79	This work

Table S2. Comparison of BET surface area and pore volume of Cu^{n+}SSZ-13-190-R before and after NO_2 dynamic column adsorption.

Cu^{n+}SSZ-13-190-R	BET surface area (m^2/g)	Total pore volume (cm^3/g)
Before NO_2 adsorption	557.97	0.34
After NO_2 adsorption	579.53	0.40

Table S3. Electron occupancy in outer-shell orbitals of N, O and transition metal ions before and after NO_2 adsorption (Lowdin).

	N-2s	*N-2pz*	*N-2px*	*N-2py*	*O-2s*	*O-2pz*	*O-2px*	*O-2py*	*O-2s*	*O-2pz*	*O-2px*	*O-2py*	*Cu-3dz2*	*Cu-3dzx*	*Cu-3dzy*	*Cu-3dx2-y2*	*Cu-3dxy*	*Cu-4s*	*Cu-4pz*	*Cu-4px*	*Cu-4py*
NO_2	1.28	0.91	1.09	1.21	1.75	1.40	1.48	1.51	1.75	1.34	1.49	1.55									
NO	1.71	1.10	1.03	1.03	1.71	1.38	1.44	1.44													
Cu^+													1.97	2.03	2.05	1.78	2.01	0.44	0.10	0.24	0.21
$Cu^+ + NO_2$	1.19	1.23	1.01	1.05	1.74	1.63	1.36	1.39	1.74	1.52	1.41	1.43	1.60	1.99	1.97	1.94	2.01	0.43	0.26	0.25	0.23
$Cu^+ + NO$	1.43	1.20	1.08	1.09	1.70	1.49	1.40	1.39					1.95	1.85	1.88	1.93	1.95	0.49	0.26	0.20	0.20
Cu^{2+}													1.98	2.03	2.02	1.52	2.00	0.41	0.12	0.24	0.24
$Cu^{2+} + NO_2$	1.18	1.22	1.00	1.06	1.74	1.60	1.35	1.41	1.73	1.53	1.40	1.41	1.64	1.94	1.96	1.98	2.00	0.42	0.26	0.26	0.23
$Cu^{2+} + NO$	1.49	1.06	1.00	1.10	1.69	1.39	1.37	1.38					1.81	1.84	1.85	1.99	1.97	0.42	0.31	0.24	0.23

References

1. Kim, Y.; Hwang, S.; Lee, J.; Ryou, Y.; Lee, H.; Kim, C. H.; Kim, D. H., Comparison of NOx Adsorption/Desorption Behaviors over Pd/CeO_2 and Pd/SSZ-13 as Passive NOx Adsorbers for Cold Start Application. *Emission Control Science and Technology* **2019,** *5* (2), 172-182.
2. Colombo, M.; Nova, I.; Tronconi, E., NO2 adsorption on Fe- and Cu-zeolite catalysts: The effect of the catalyst red–ox state. *Applied Catalysis B: Environmental* **2012,** *111-112*, 433-444.